Coligand-driven modulation of magnetic property in trigonal prismatic cobalt(II) single-ion magnets

Aoyun Zhang,[a] Chennan Zhang,[a] Junnan Qiao,[a] Yawen Wang,[a] Ulli Englert,[a] Lei Chen,*[a] Shu-Chang Luo,*[b] Zhao-Yang Li,*[c] and Li-Zhuang Chen*[a]

[a]*School of Environmental and Chemical Engineering, Jiangsu University of Science and Technology, Zhenjiang 212100, China*
[b]*School of Chemical Engineering, Guizhou University of Engineering Science, Bijie 551700, China*
[c]*School of Materials Science and Engineering, Nankai University, Tianjin 300350, China*

Electronic Supplementary Information

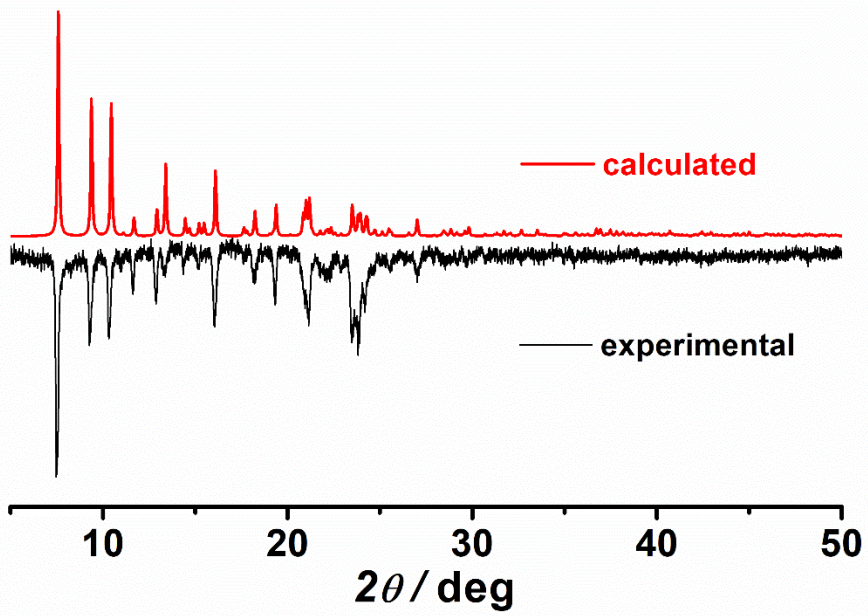

Figure S1. PXRD pattern for complex **1**.

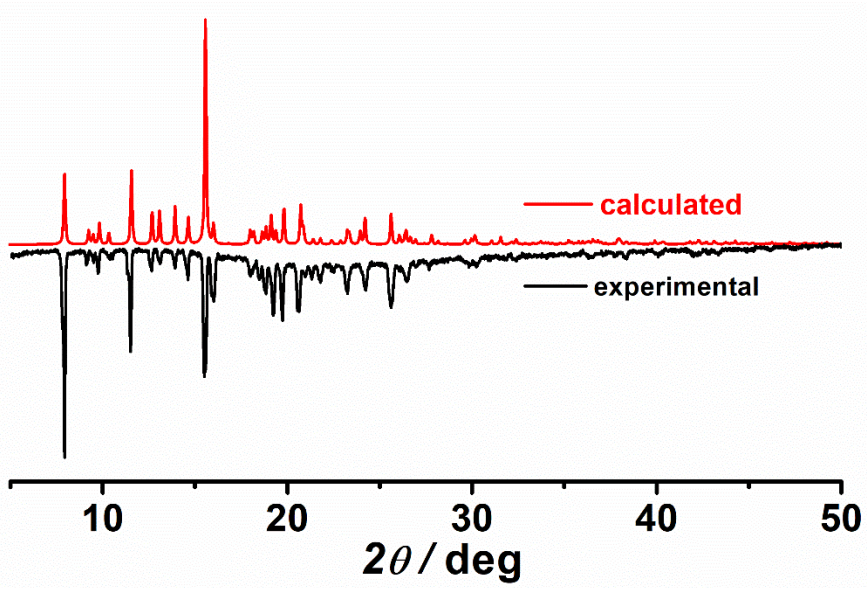

Figure S2. PXRD pattern for complex **2**.

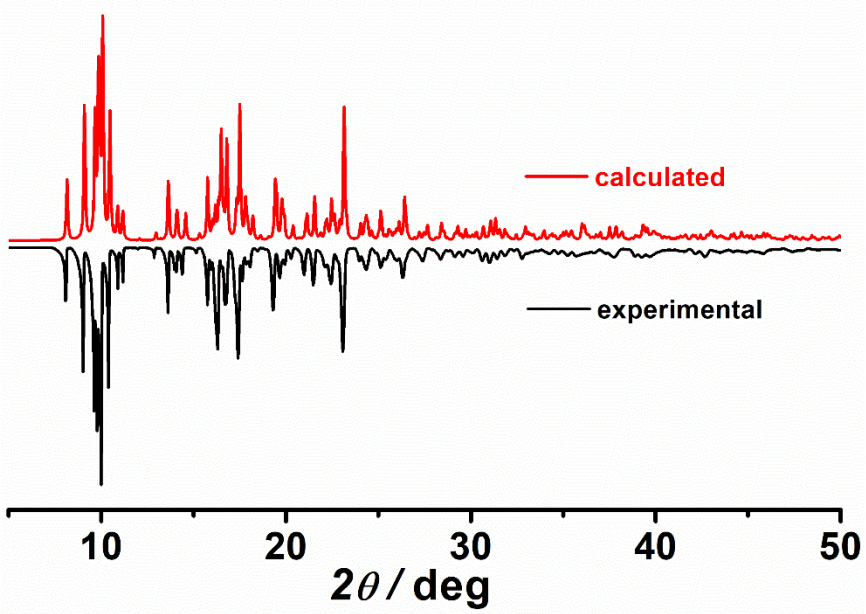

Figure S3. PXRD pattern for complex **3**.

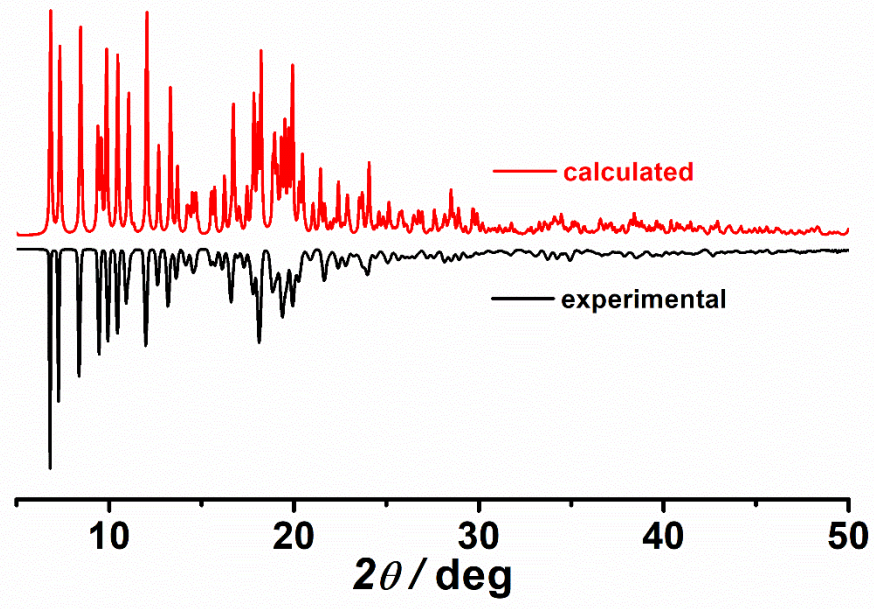

Figure S4. PXRD pattern for complex **4**.

Table S1. Crystal data and structure refinement for complexes **1**−**4**.

	1	**2**	**3**	**4**
Molecular formula	$C_{36}H_{44}CoN_6O_6$	$C_{38}H_{47}CoF_6N_4O_2P$	$C_{44}H_{56}CoN_4O_7$	$C_{62}H_{68}BCoN_5O_2$
CCDC no	2450168	2519785	2450170	2450169
Formula weight	715.70	795.69	811.85	984.95
Temperature / K	293(2)	296(2)	296(2)	193(2)
Wavelength / Å	0.71073	0.71073	0.71073	0.71073
crystal system	Orthorhombic	Orthorhombic	Triclinic	Triclinic
Space group	*P*nma	*P*nma	*P*-1	*P*-1
a / Å	23.2807(8)	22.0009(19)	10.3618(9)	11.0663(7)
b / Å	16.0259(4)	16.9470(16)	11.5594(8)	13.5600(9)
c / Å	9.9543(3)	10.4762(10)	18.3520(16)	19.0783(12)
α / deg	90	90	94.555(6)	101.680(3)
β / deg	90	90	90.894(7)	103.827(3)
γ / deg	90	90	109.837(6)	99.809(3)
V / Å^3	3713.89(19)	3906.0(6)	2059.0(3)	2649.3(3)
Z	4	4	2	2
D_{calc}, Mg/m^3	1.280	1.353	1.309	1.235
μ / mm^{-1}	0.513	0.547	0.472	0.373
F (000)	1508	1660	862	1046
Goodness-of-fit on F^2	1.056	1.626	0.877	1.085
Final R indices [$I > 2\sigma(I)$][a]	R1 = 0.0602, wR2 = 0.1679	R1 = 0.1101, wR2 = 0.3270	R1 = 0.0791, wR2 = 0.1953	R1 = 0.1127, wR2 = 0.3356
R indices (all data)[a]	R1 = 0.0732, wR2 = 0.1793	R1 = 0.1411, wR2 = 0.3522	R1 = 0.1553, wR2 = 0.2247	R1 = 0.1327, wR2 = 0.3505

[a] $wR_2 = [\Sigma[w(F_o^2-F_c^2)^2]/\Sigma[w(Fo^2)^2]]^{1/2}$, $R_1 = \Sigma||F_o|-|F_c||/\Sigma|F_o|$.

Table S2. Selected bond lengths (Å) and angles (°) for complexes **1**−**4**.

1		**2**		**3**		**4**	
Co1-N1	2.193(3)	Co1-N1	2.200(5)	Co1-N1	2.260(5)	Co1-N1	2.226(6)
Co1-N1A	2.193(3)	Co1-N1A	2.200(5)	Co1-N2	2.264(5)	Co1-N2	2.374(5)
Co1-N2	2.192(3)	Co1-N2	2.190(5)	Co1-N3	2.248(5)	Co1-N3	2.226(5)
Co1-N2A	2.192(3)	Co1-N2A	2.190(5)	Co1-N4	2.267(5)	Co1-N4	2.331(6)
Co1-O1	2.131(4)	Co1-O1	2.154(7)	Co1-O1	2.072(4)	Co1-O1	2.019(5)
Co1-O2	2.232(3)	Co1-O2	2.180(7)	Co1-O2	2.066(4)	Co1-O2	2.081(5)
Average Co-O length	**2.182**		**2.167**		**2.069**		**2.050**
N1-Co1-N2	80.36(12)	N1-Co1-N2	81.1(2)	N1-Co1-N4	77.4(2)	N1-Co1-N2	76.5(2)
N1A-Co1-N2A	80.36(12)	N1A-Co1-N2A	81.1(2)	N2-Co1-N3	78.5(2)	N3-Co1-N4	77.3(2)
O1-Co1-O2	58.12(15)	O1-Co1-O2	59.8(3)	O1-Co1-O2	76.64(15)	O1-Co1-O2	76.84(19)

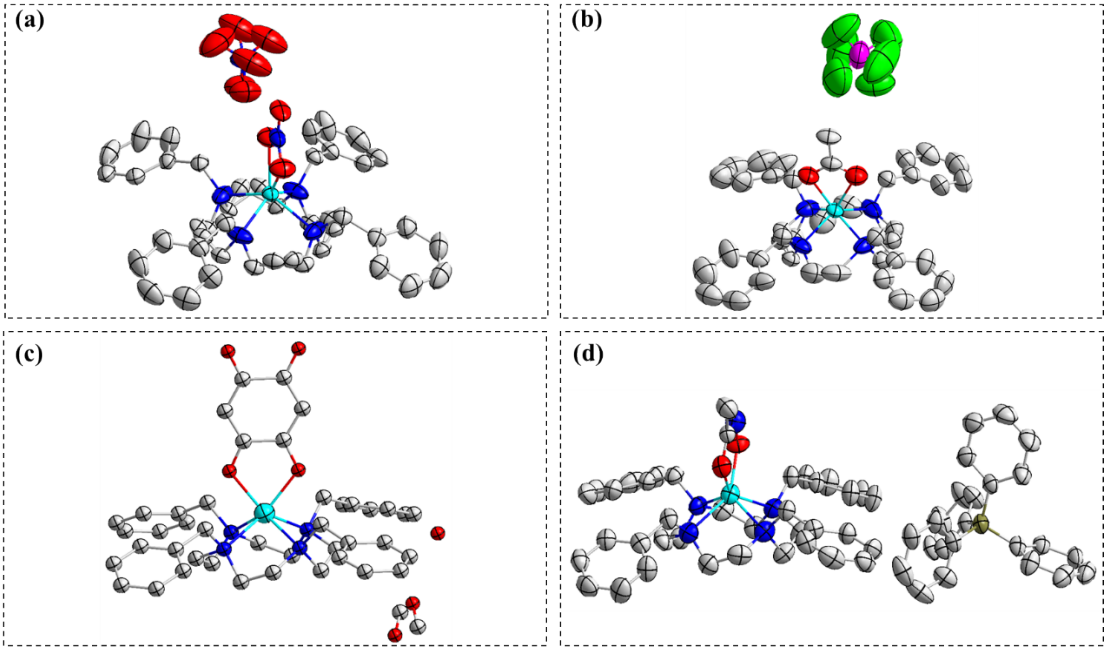

Figure S5. ORTEP drawing of crystal structures for complexes **1** (a), **2** (b), **3** (c) and **4** (d). Cyan, red, blue, dark yellow, green and pink spheres represent Co, O, N, B, F and P atoms, respectively. H atoms are omitted for clarity.

Table S3. Continuous shape measure (CSM) analyses of six-coordinate geometries for complexes **1**−**4** by SHAPE software.

Six-coordination	**1**	**2**	**3**	**4**
Hexagon	33.486	32.646	33.504	33.838
Pentagonal pyramid	15.257	15.760	14.379	14.253
Octahedron	17.485	17.439	15.459	14.662
Trigonal prism	1.425	1.311	0.468	0.652

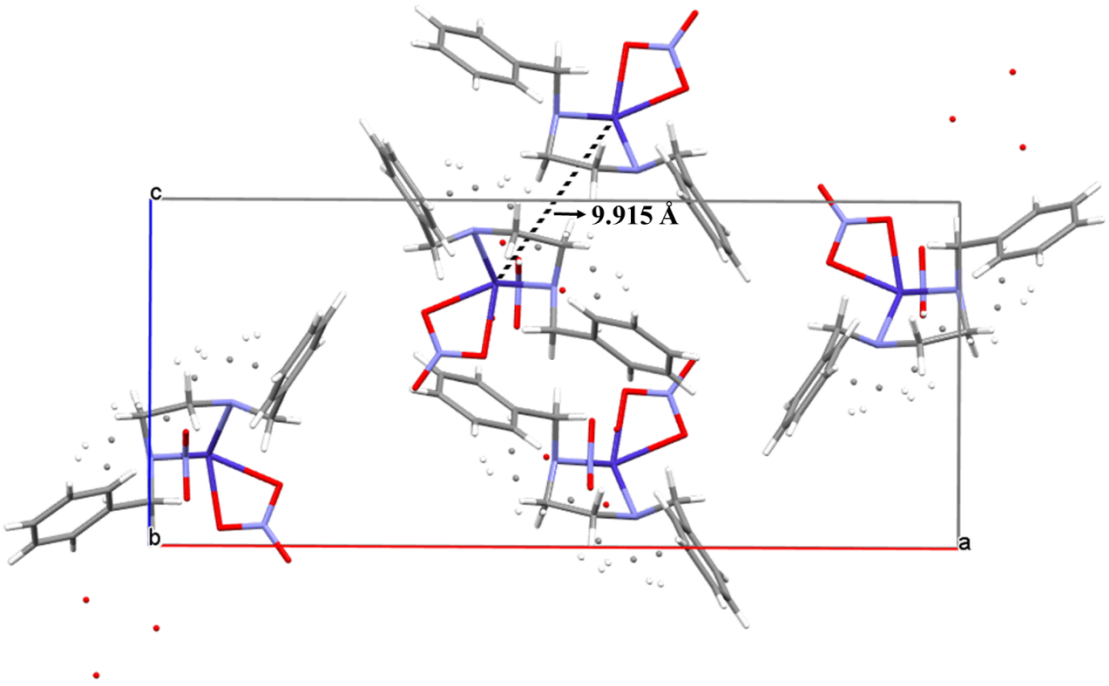

Figure S6. Stacking between adjacent complexes in the unit cell of **1**.

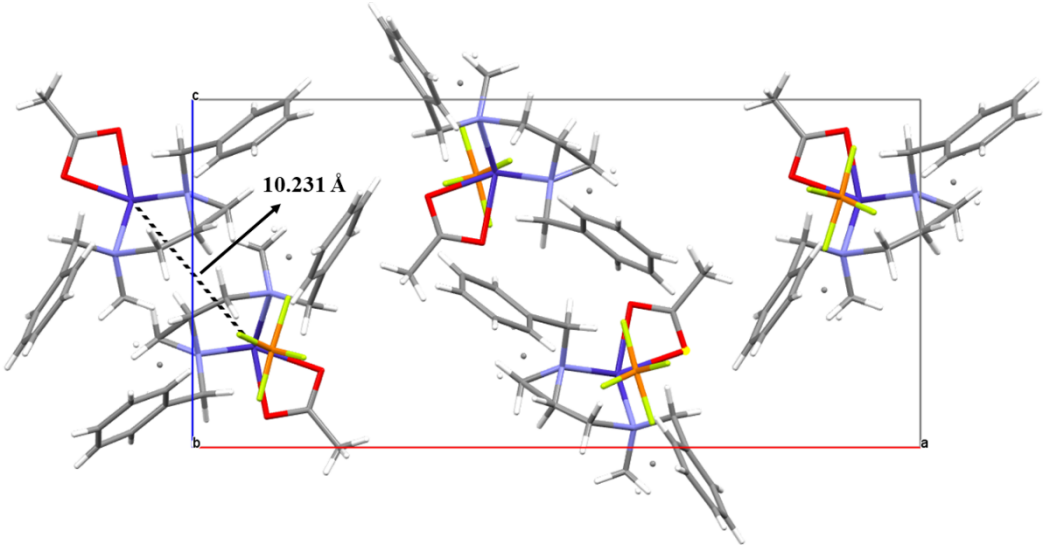

Figure S7. Stacking between adjacent complexes in the unit cell of **2**.

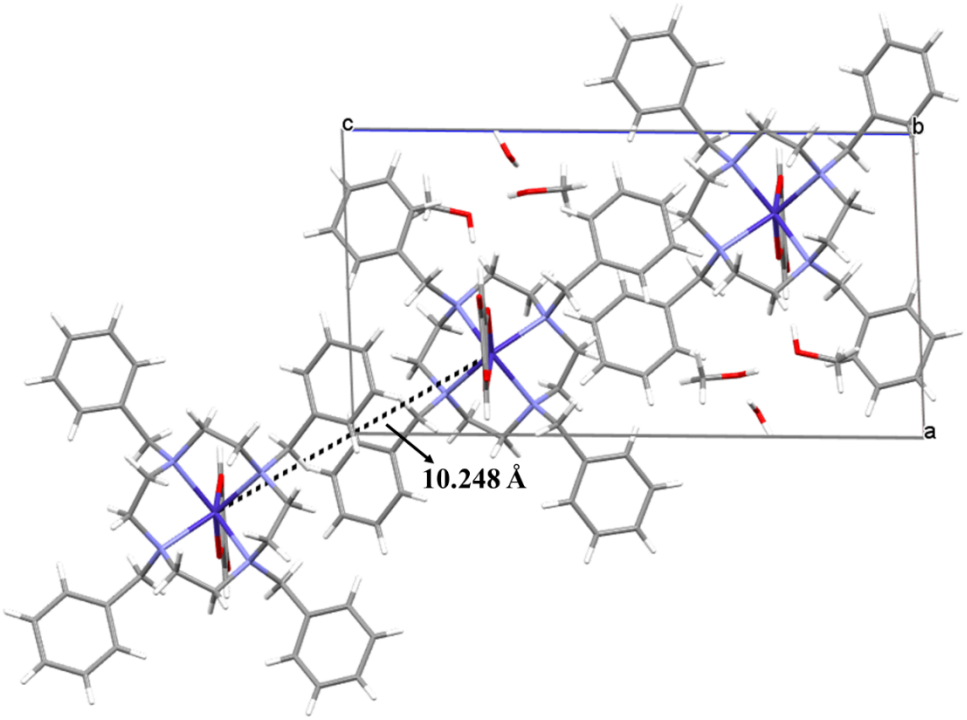

Figure S8. Stacking between adjacent complexes in the unit cell of **3**.

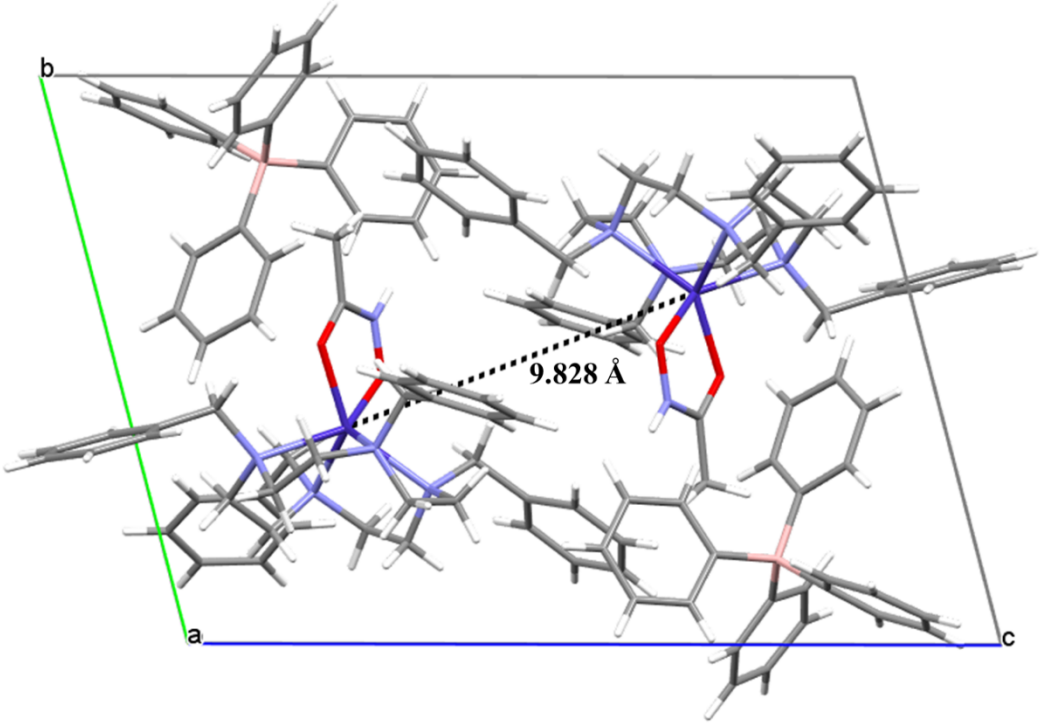

Figure S9. Stacking between adjacent complexes in the unit cell of **4**.

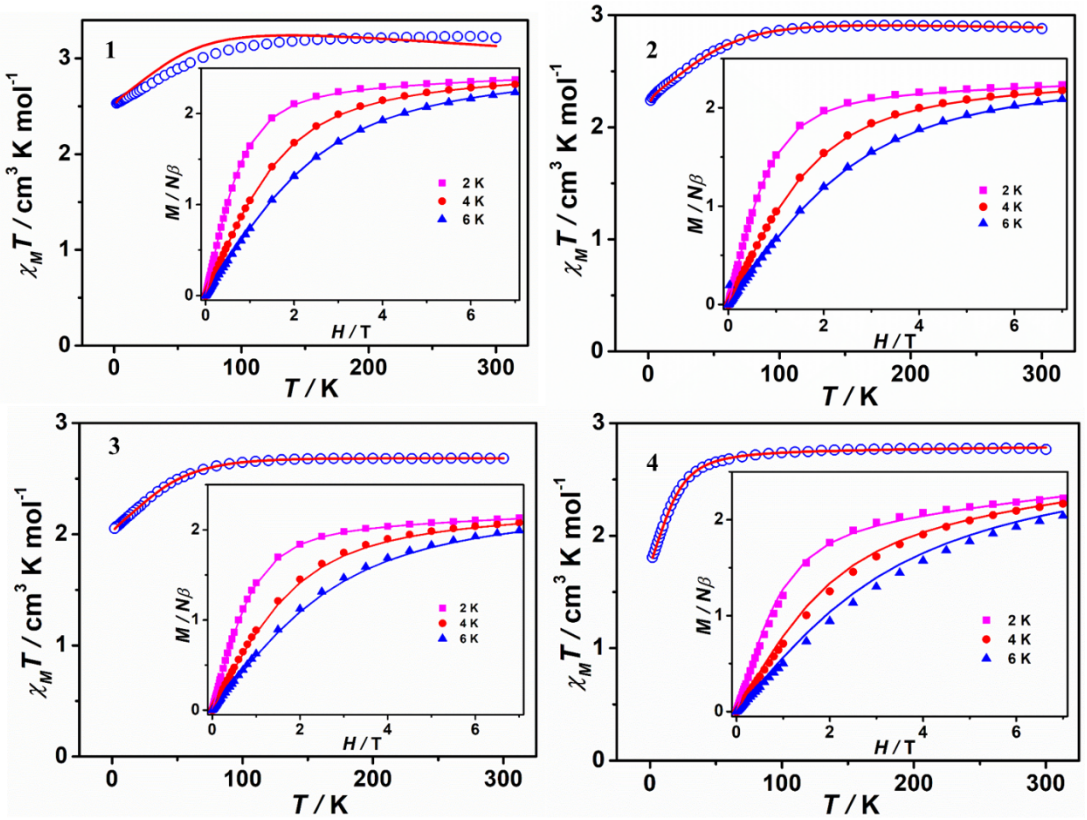

Figure S10. Temperature dependence of the dc magnetic susceptibility for complexes **1**–**4**. Inset: variable temperature and field dc magnetization data for complexes **1**–**4**. Solid lines represent the best fits with the PHI program.

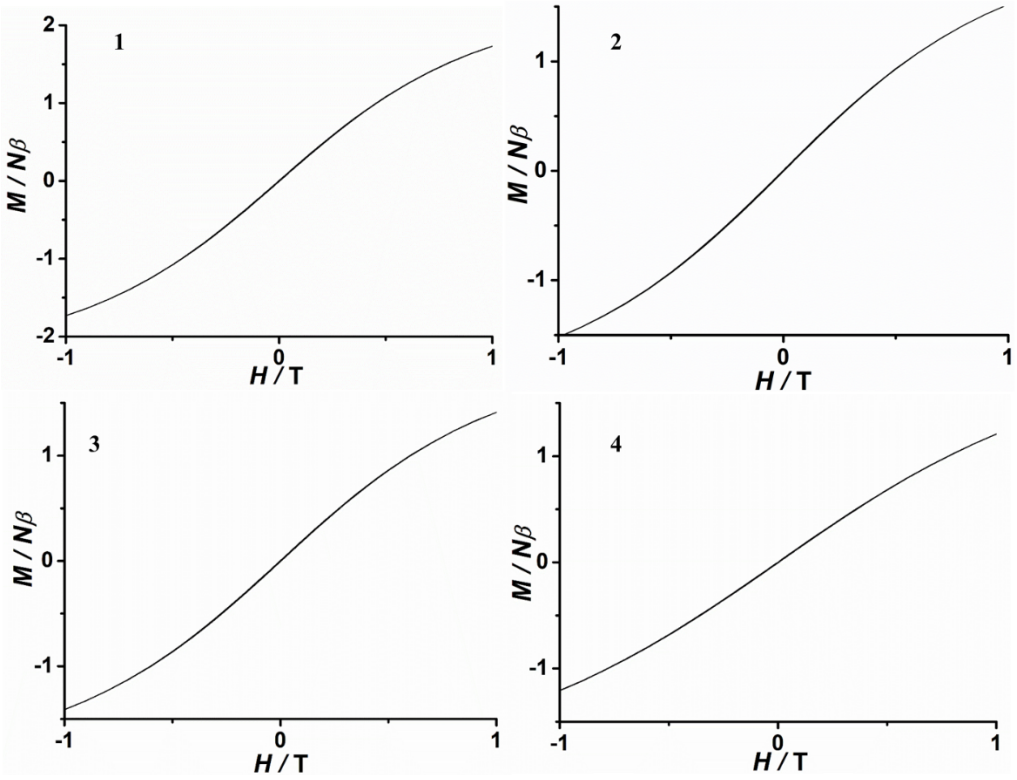

Figure S11. Variable-field magnetization data for complexes **1**–**4** at a sweep rate of 200 Oe s^{-1} at 2 K.

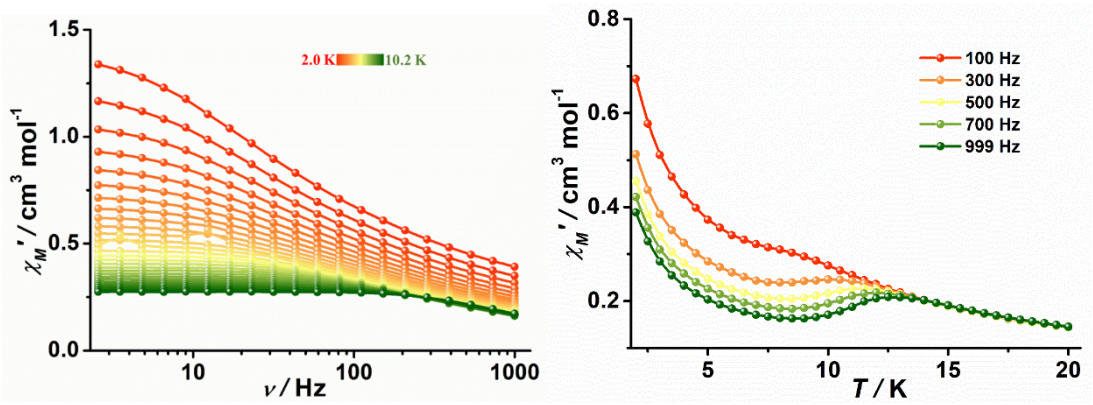

Figure S12. Frequency (left) and temperature-dependence (right) of in-phase (χ_M') ac susceptibility for complex **1** under 0 Oe dc field. Solid lines are intended to guide the eye.

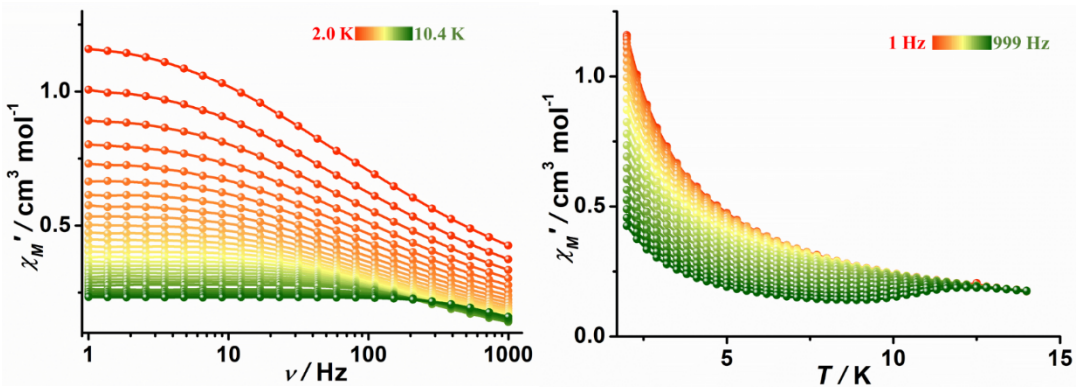

Figure S13. Frequency- (left) and temperature-dependence (right) of in-phase (χ_M') ac susceptibility for complex **2** under 0 Oe dc field. Solid lines are intended to guide the eye.

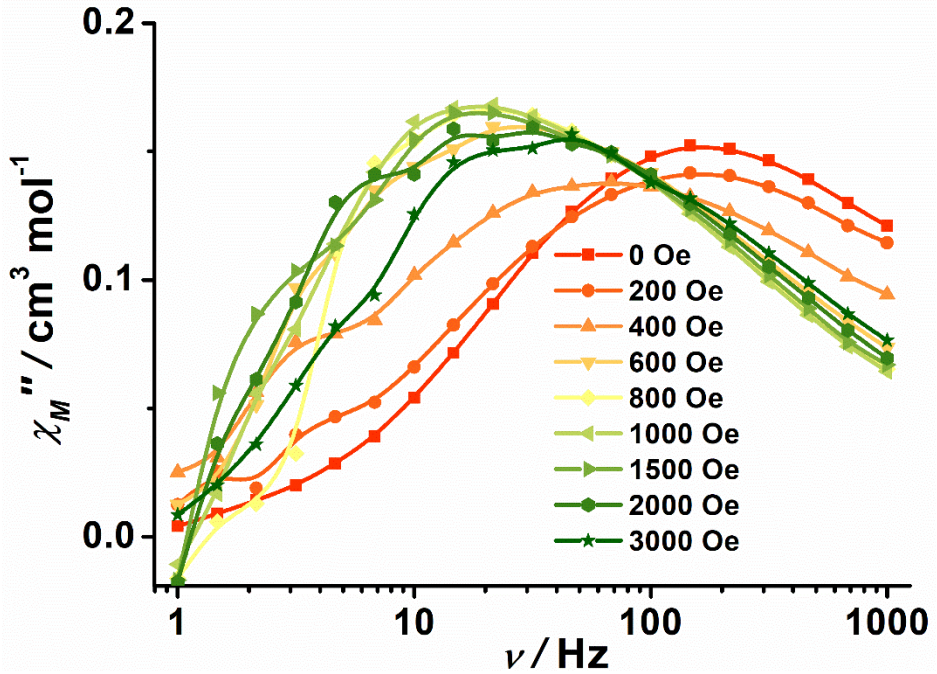

Figure S14. Field dependence of out-of-phase ac susceptibility (χ_M'') for complex **1** at 4 K. Solid lines are intended to guide the eye.

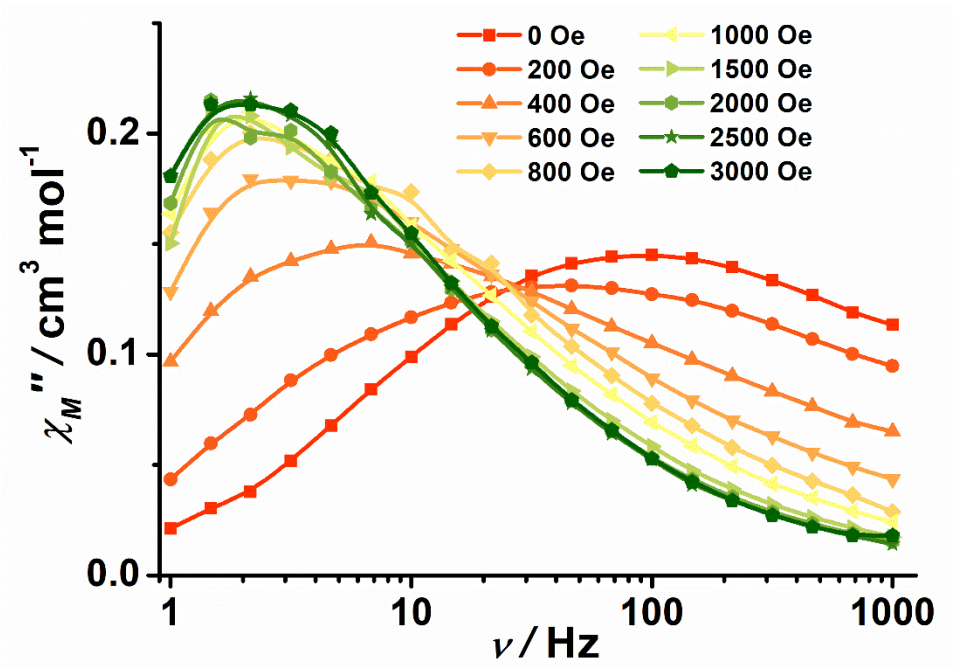

Figure S15. Field dependence of out-of-phase ac susceptibility (χ_M'') for complex **2** at 3 K. Solid lines are intended to guide the eye.

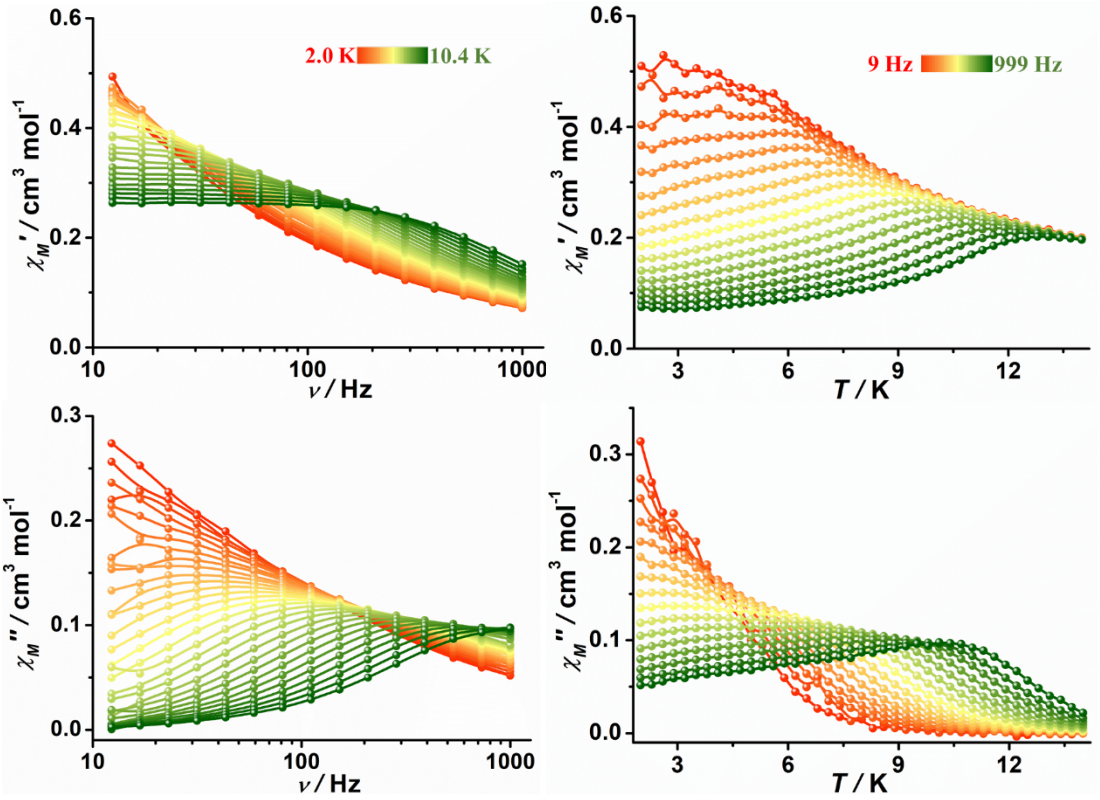

Figure S16. Frequency- (left) and temperature-dependence (right) of in-phase (χ_M') and out-of-phase (χ_M'') ac susceptibilities for complex **1** under 1000 Oe dc field. Solid lines are intended to guide the eye.

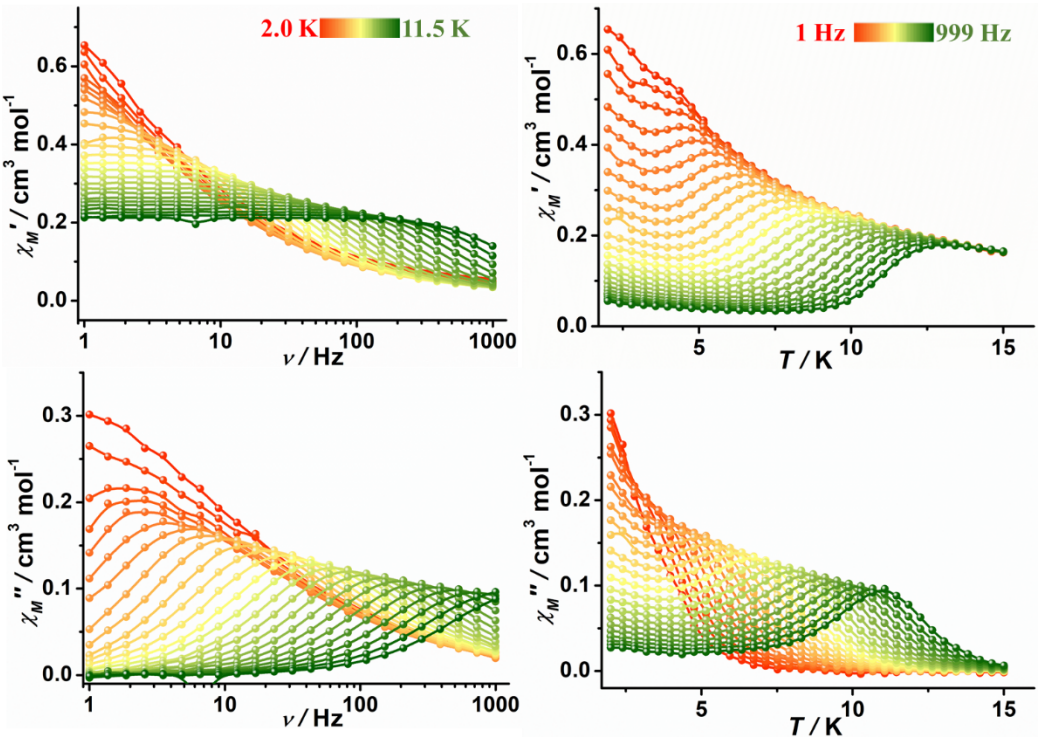

Figure S17. Frequency- (left) and temperature-dependence (right) of in-phase (χ_M') and out-of-phase (χ_M'') ac susceptibilities for complex **2** under 3000 Oe dc field. Solid lines are intended to guide the eye.

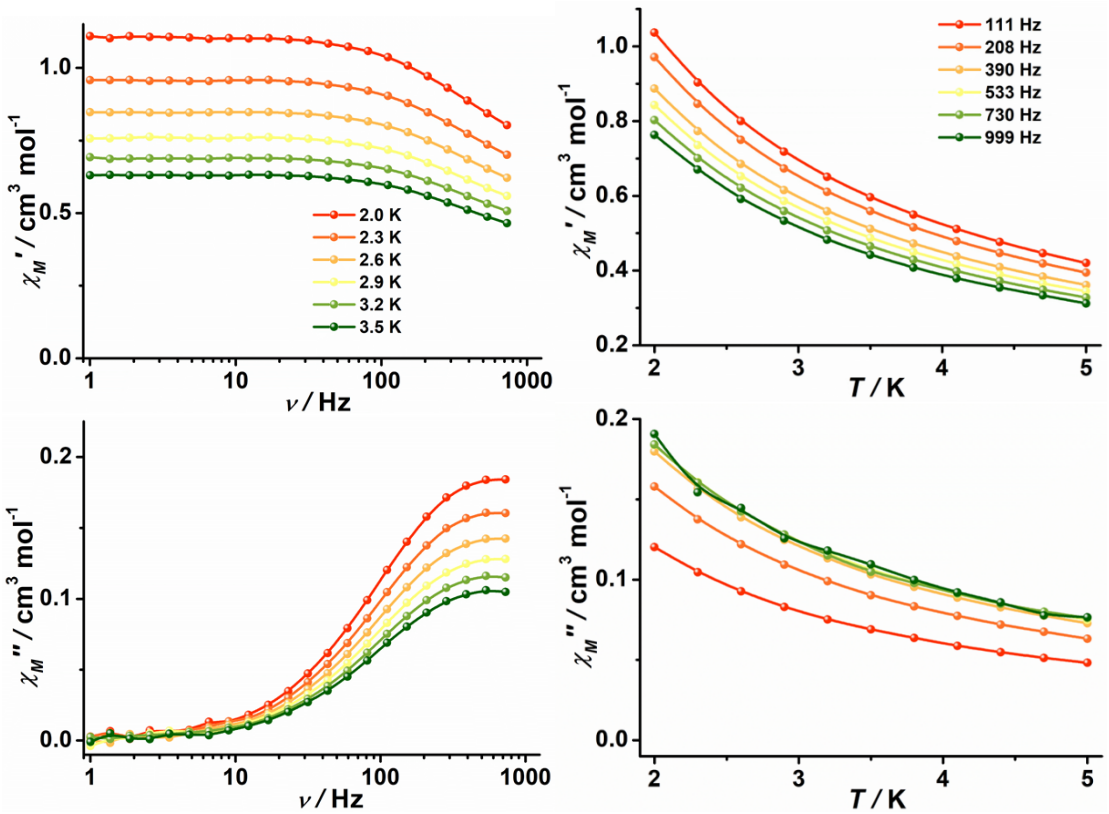

Figure S18. Frequency- and temperature-dependence of in-phase (χ_M') and out-of-phase (χ_M'') ac susceptibilities for complex **3** under 0 Oe dc field. Solid lines are intended to guide the eye.

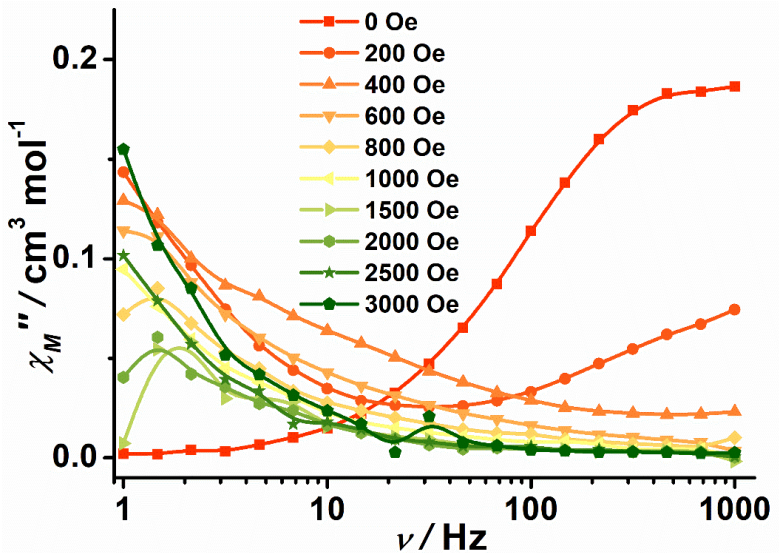

Figure S19. Field dependence of out-of-phase ac susceptibility (χ_M'') for complex **3** at 2 K. Solid lines are intended to guide the eye.

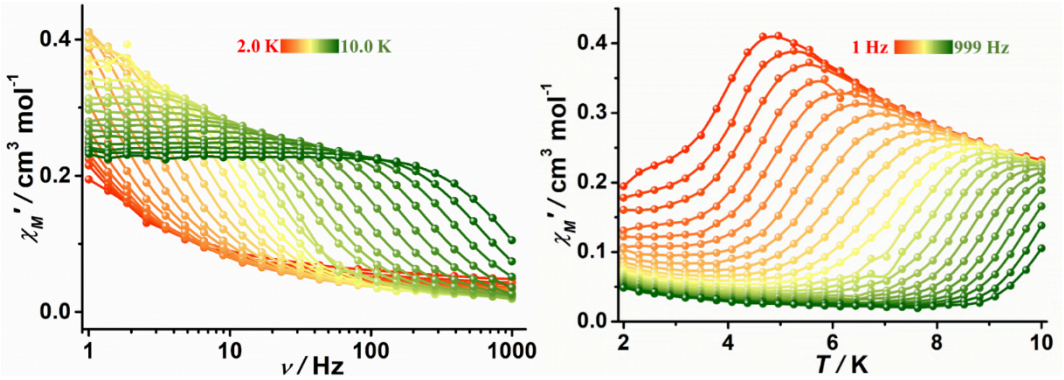

Figure S20. Frequency- (left) and temperature-dependence (right) of in-phase (χ_M') ac susceptibility for complex **3** under 800 Oe dc field. Solid lines are intended to guide the eye.

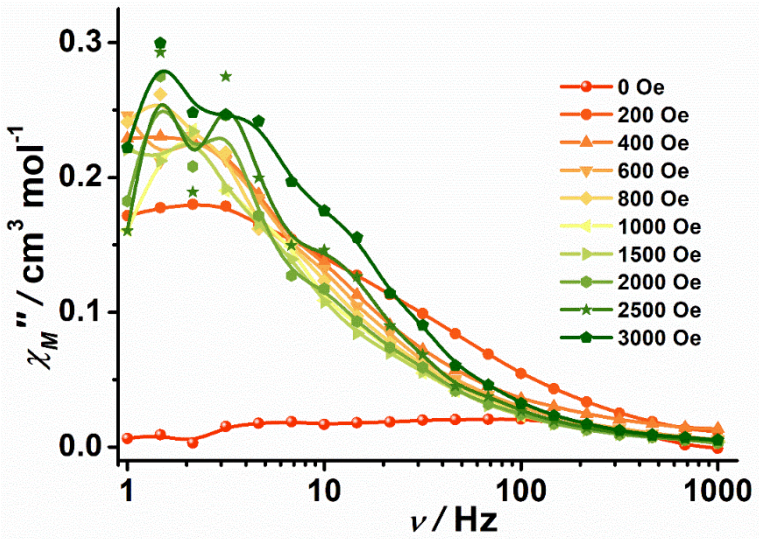

Figure S21. Field dependence of out-of-phase ac susceptibility (χ_M'') for complex **4** at 2 K. Solid lines are intended to guide the eye.

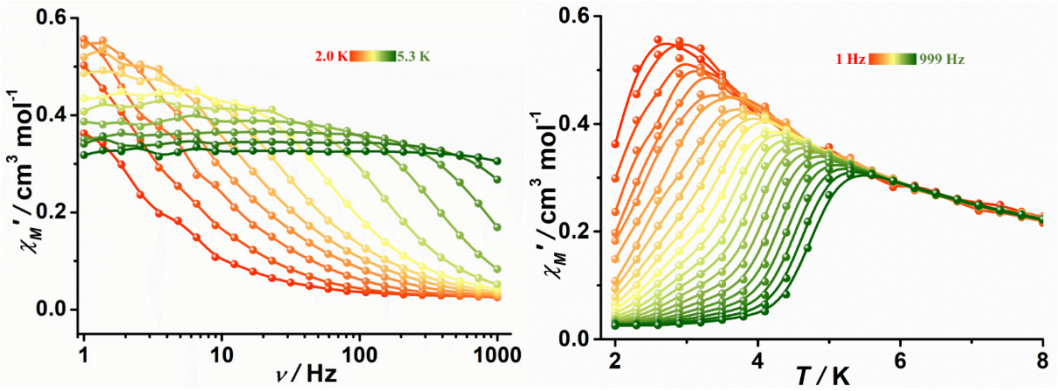

Figure S22. Frequency- (left) and temperature-dependence (right) of in-phase (χ_M') ac susceptibility for complex **4** under 800 Oe dc field. Solid lines are intended to guide the eye.

Table S4. Parameters obtained by fitting the Cole-Cole plot under 0 Oe dc field for complex **1**.

T / K	χ_S	χ_T	τ	a
2	0.28091	1.51207	0.00462	0.43
2.3	0.24094	1.30202	0.0038	0.43
2.6	0.21103	1.14298	0.00317	0.43
2.9	0.18679	1.01872	0.00268	0.43
3.2	0.16768	0.91865	0.00230	0.42
3.5	0.15402	0.83616	0.00199	0.42
3.8	0.14152	0.76695	0.00173	0.42
4.1	0.13400	0.70865	0.00155	0.41
4.4	0.12685	0.66025	0.00139	0.40
4.7	0.12088	0.61377	0.00122	0.39
5	0.12194	0.57949	0.00116	0.38
5.3	0.11390	0.54107	0.001	0.37
5.6	0.10185	0.52518	9.33363×10^{-4}	0.39
5.9	0.11039	0.48324	8.33995×10^{-4}	0.34
6.2	0.10867	0.45834	7.57149×10^{-4}	0.32
6.5	0.10871	0.43603	6.99794×10^{-4}	0.30
6.8	0.10775	0.41632	6.39544×10^{-4}	0.28
7.1	0.10547	0.39685	5.76364×10^{-4}	0.26
7.4	0.10561	0.38061	5.30891×10^{-4}	0.23
7.7	0.10477	0.36530	4.81895×10^{-4}	0.21
8	0.10175	0.35092	4.31191×10^{-4}	0.19
8.3	0.10034	0.33766	3.88625×10^{-4}	0.17
8.7	0.09841	0.32530	3.47631×10^{-4}	0.15
9	0.09565	0.31424	3.09029×10^{-4}	0.14
9.3	0.09546	0.30389	2.78042×10^{-4}	0.12
9.6	0.09165	0.29429	2.43295×10^{-4}	0.11
9.9	0.09042	0.28501	2.15803×10^{-4}	0.09
10.2	0.08830	0.27672	1.89016×10^{-4}	0.07

Table S5. Parameters obtained by fitting the Cole-Cole plot under 1000 Oe dc field for complex **1**.

T / K	χ_S	χ_T	τ	a
2	0.02025	1.56525	0.06094	0.50
2.3	0.02021	1.27887	0.03436	0.48
2.6	0.0112	1.1224	0.02415	0.49
2.9	0.00242	1.23512	0.03234	0.52
3.2	~0	1.08943	0.02265	0.52
3.5	~0	0.97474	0.0156	0.51
3.8	~0	0.83015	0.00903	0.49
4.1	~0	0.75940	0.00654	0.48
4.4	~0	0.76298	0.00675	0.50
4.7	~0	0.68690	0.00472	0.48
5	~0	0.63619	0.00357	0.47
5.3	~0	0.61392	0.00306	0.46
5.6	~0	0.56799	0.0023	0.45
5.9	~0	0.53369	0.00181	0.43
6.2	~0	0.50140	0.00143	0.41
6.5	~0	0.47120	0.00113	0.39
6.8	~0	0.44623	9.3835×10^{-4}	0.38
7.1	~0	0.42224	7.53722×10^{-4}	0.36
7.4	~0	0.39859	6.17229×10^{-4}	0.34
7.7	~0	0.37916	5.10925×10^{-4}	0.32
8	~0	0.36250	4.33484×10^{-4}	0.30
8.3	~0	0.34669	3.66993×10^{-4}	0.28
8.6	~0	0.33130	3.11805×10^{-4}	0.26
8.9	~0	0.31878	2.67669×10^{-4}	0.24
9.2	~0	0.30664	2.30117×10^{-4}	0.22
9.5	~0	0.29560	1.98695×10^{-4}	0.20
9.8	~0	0.28635	1.70964×10^{-4}	0.19
10.1	~0	0.27641	1.48375×10^{-4}	0.17
10.4	~0	0.26757	1.27909×10^{-4}	0.15

Table S6. Parameters obtained by fitting the Cole-Cole plot under 0 Oe dc field for complex **2**.

T / K	χ_S	χ_T	τ	a
2	0.23713	1.23185	0.00186	0.48
2.3	0.21143	1.06501	0.00172	0.47
2.6	0.191	0.94222	0.00161	0.46
2.9	0.17461	0.84314	0.00151	0.45
3.2	0.16216	0.76407	0.00143	0.44
3.5	0.15267	0.69763	0.00135	0.43
3.8	0.14349	0.64276	0.00128	0.42
4.1	0.13625	0.59554	0.00121	0.41
4.4	0.13103	0.55441	0.00115	0.39
4.7	0.12696	0.51827	0.00109	0.38
5	0.12126	0.48725	0.00102	0.36

5.3	0.11805	0.46004	9.67779E-4	0.35
5.6	0.1163	0.43377	9.08636E-4	0.33
5.9	0.11366	0.41162	8.53983E-4	0.31
6.2	0.11067	0.39135	7.95588E-4	0.29
6.5	0.10837	0.37299	7.40139E-4	0.27
6.8	0.10659	0.35648	6.89675E-4	0.25
7.1	0.10279	0.34227	6.29665E-4	0.24
7.4	0.10177	0.32755	5.80568E-4	0.22
7.7	0.09885	0.3144	5.27318E-4	0.20
8	0.09523	0.30243	4.72834E-4	0.18
8.3	0.09566	0.29163	4.3356E-4	0.16
8.6	0.0934	0.28111	3.85402E-4	0.14
8.9	0.08986	0.27142	3.37755E-4	0.12
9.2	0.08511	0.26324	2.91806E-4	0.11
9.5	0.08352	0.25473	2.5335E-4	0.10
9.8	0.07948	0.24709	2.15335E-4	0.08
10.1	0.079	0.23968	1.85648E-4	0.06
10.4	0.07645	0.23306	1.55427E-4	0.06

Table S7. Parameters obtained by fitting the Cole-Cole plot under 3000 Oe dc field for complex **2**.

T / K	χ_S	χ_T	τ	a
2	0.02511	1.53795	0.26451	0.51
2.4	0.0207	1.31735	0.19692	0.51
2.8	0.02568	1.01215	0.09914	0.48
3.2	0.03003	0.88296	0.07227	0.45
3.6	0.03252	0.7746	0.05094	0.41
4.0	0.03561	0.67541	0.03439	0.37
4.4	0.03759	0.6033	0.02423	0.32
4.8	0.03954	0.53438	0.01664	0.27
5.2	0.03911	0.48436	0.01202	0.23
5.5	0.0388	0.43902	0.00871	0.19
5.9	0.03594	0.41261	0.00669	0.17
6.3	0.03503	0.38505	0.0051	0.15
6.7	0.03373	0.36054	0.00389	0.13
7.1	0.03229	0.34074	0.00302	0.11
7.5	0.03066	0.32159	0.00232	0.09
7.9	0.02921	0.30479	0.00178	0.08
8.3	0.02835	0.29053	0.00138	0.07
8.7	0.02676	0.27772	0.00105	0.06
9.1	0.0253	0.26529	7.84718E-4	0.05
9.5	0.02445	0.25486	5.88979E-4	0.05
9.9	0.02222	0.2455	4.33426E-4	0.05
10.3	0.023	0.23597	3.20352E-4	0.04
10.7	0.02424	0.22701	2.35368E-4	0.03
11.1	0.02434	0.21873	1.72881E-4	0.02

11.5	0.03065	0.21141	1.30932E-4	0.01

Table S8. Parameters obtained by fitting the Cole-Cole plot under 800 Oe dc field for complex **3**.

T / K	χ_S	χ_T	τ	a
3.2	0.04765	790.1	334109	0.44
3.5	0.04002	587.361	269094	0.46
3.8	0.03463	477.316	242686	0.47
4.1	0.03055	522.055	250874	0.47
4.4	0.0342	1.11963	0.9249	0.36
4.7	0.03294	0.92218	0.51827	0.33
5	0.03176	0.79561	0.30001	0.29
5.3	0.03133	0.65073	0.15925	0.24
5.6	0.03134	0.57106	0.09832	0.20
5.9	0.0309	0.51661	0.06537	0.16
6.1	0.03042	0.46894	0.04468	0.13
6.4	0.0286	0.43933	0.03238	0.11
6.7	0.02773	0.41573	0.02404	0.10
7.0	0.02704	0.38811	0.01778	0.08
7.3	0.02767	0.36608	0.01328	0.06
7.6	0.0243	0.35037	0.01036	0.06
7.9	0.02389	0.33636	0.00796	0.06
8.2	0.0225	0.31964	0.00634	0.04
8.5	0.02223	0.30905	0.0047	0.05
8.9	0.02098	0.29686	0.00355	0.05
9.1	0.02093	0.2852	0.00263	0.04
9.4	0.02141	0.27558	0.00191	0.03
9.7	0.02016	0.26667	0.00133	0.03
10	0.01815	0.25813	9.01847×10^{-4}	0.03

Table S9. Parameters obtained by fitting the Cole-Cole plot under 800 Oe dc field for complex **4**.

T / K	χ_S	χ_T	τ	a
2.3	0.01557	0.78921	0.08632	0.35
2.6	0.00842	0.78303	0.05215	0.40
2.9	0.02283	0.63446	0.01919	0.30
3.2	0.02921	0.56094	0.00948	0.25
3.5	0.03432	0.49668	0.00468	0.18
3.8	0.03542	0.45134	0.00226	0.12
4.1	0.03337	0.42092	0.00102	0.08
4.4	0.03092	0.3896	4.36713×10^{-4}	0.04
4.7	0.03521	0.36285	1.9497×10^{-4}	0.01
5	0.03483	0.34396	8.94321×10^{-5}	0.01

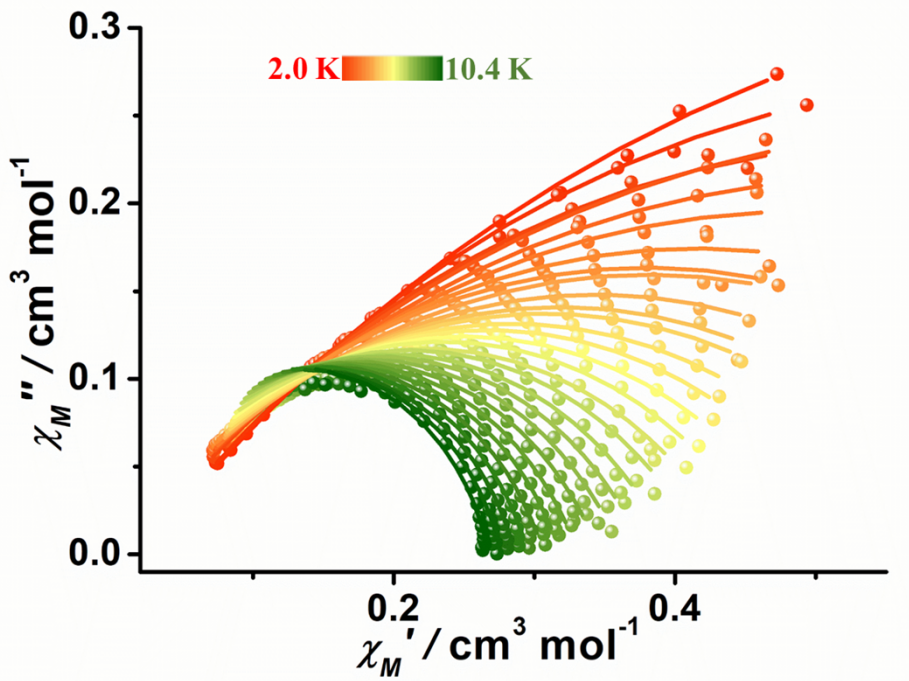

Figure S23. Cole–Cole plot of **1** under 1000 Oe DC field; solid lines are best fits to Debye's law.

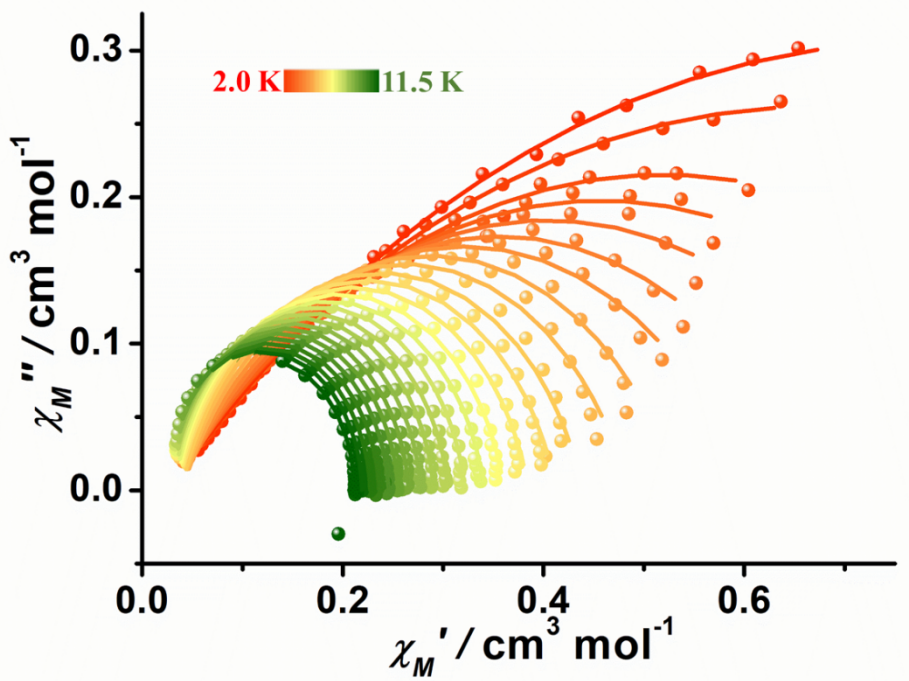

Figure S24. Cole–Cole plot of **2** under 3000 Oe DC field; solid lines are best fits to Debye's law.

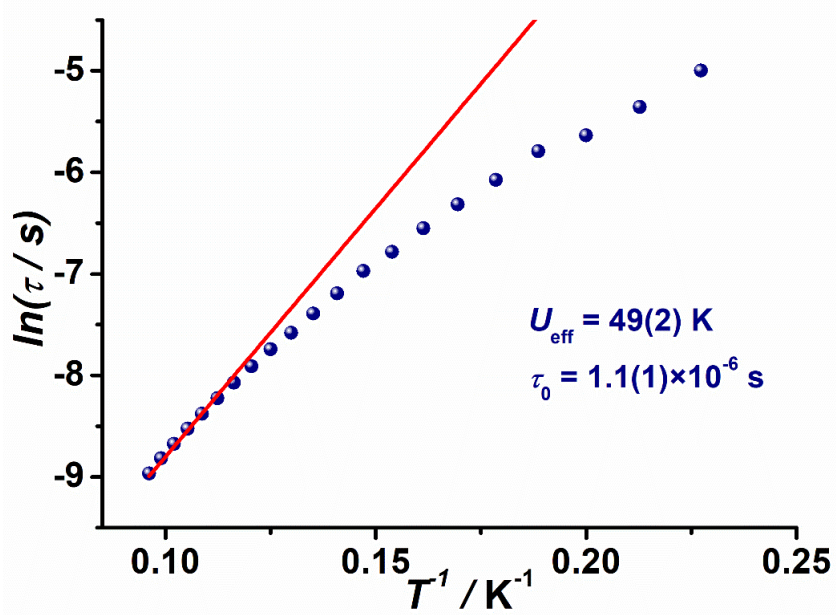

Figure S25. Relaxation time of the magnetization *ln(τ)* vs T^{-1} plot for complex **1** under 1000 Oe dc field. The red solid line represents the fit for the Orbach process.

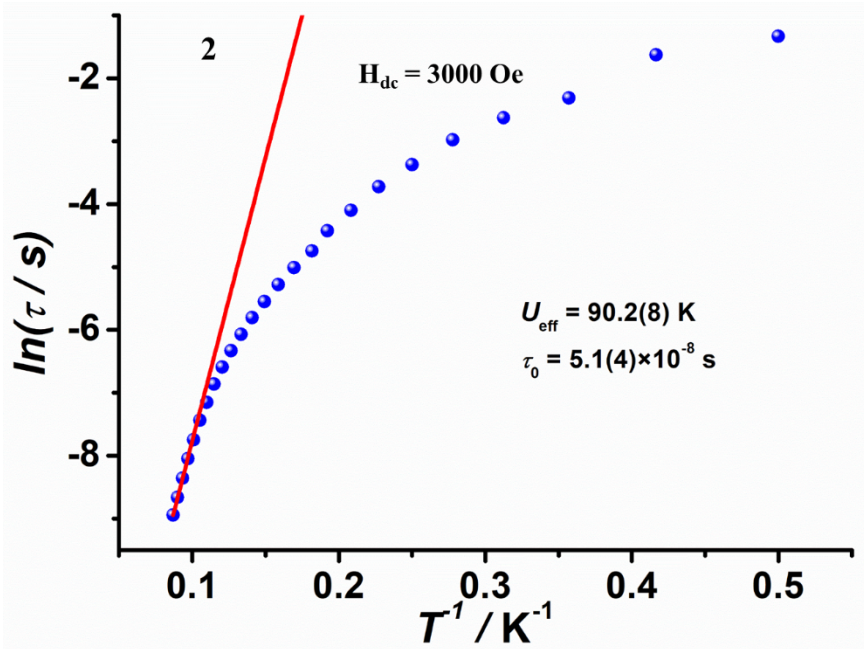

Figure S26. Relaxation time of the magnetization *ln(τ)* vs T^{-1} plot for complex **2** under 3000 Oe dc field. The red solid line represents the fit for the Orbach process.

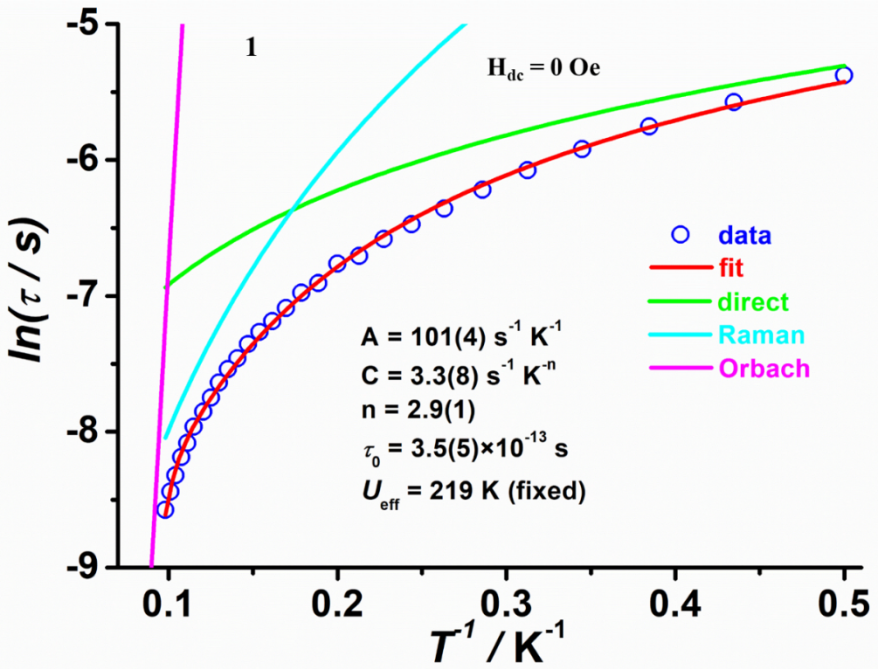

Figure S27. Relaxation time of the magnetization *ln(τ)* vs T^{-1} plot for complex **1** under 0 Oe dc field. The red solid line represents the best fit by the direct, Raman and Orbach processes. The other lines represent the individual contributions of the direct (green), Raman (cyan) and Orbach (magenta) processes.

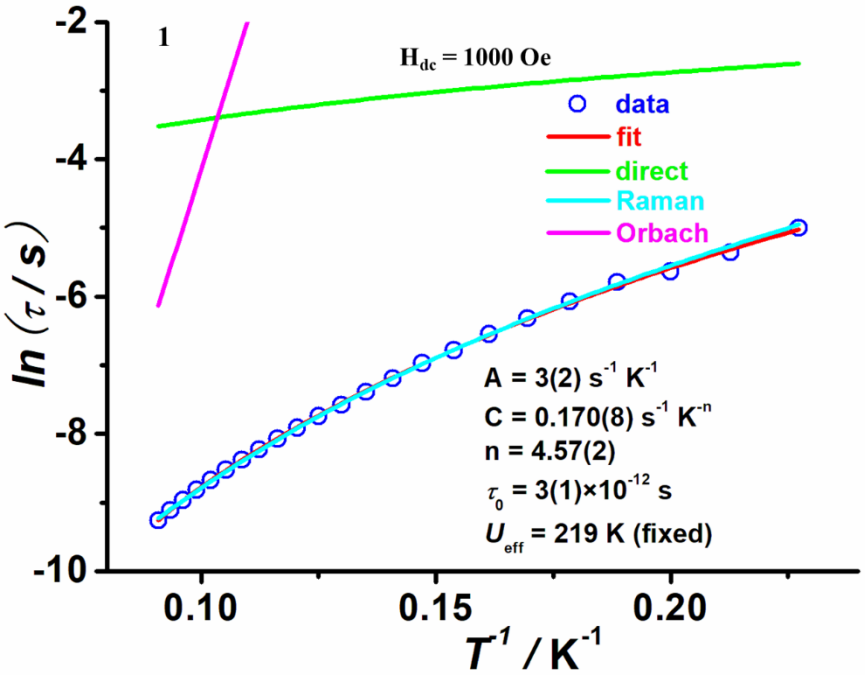

Figure S28. Relaxation time of the magnetization *ln(τ)* vs T^{-1} plot for complex **1** under 1000 Oe dc field. The red solid line represents the best fit by the direct, Raman and Orbach processes. The other lines represent the individual contributions of the direct (green), Raman (cyan) and Orbach (magenta) processes.

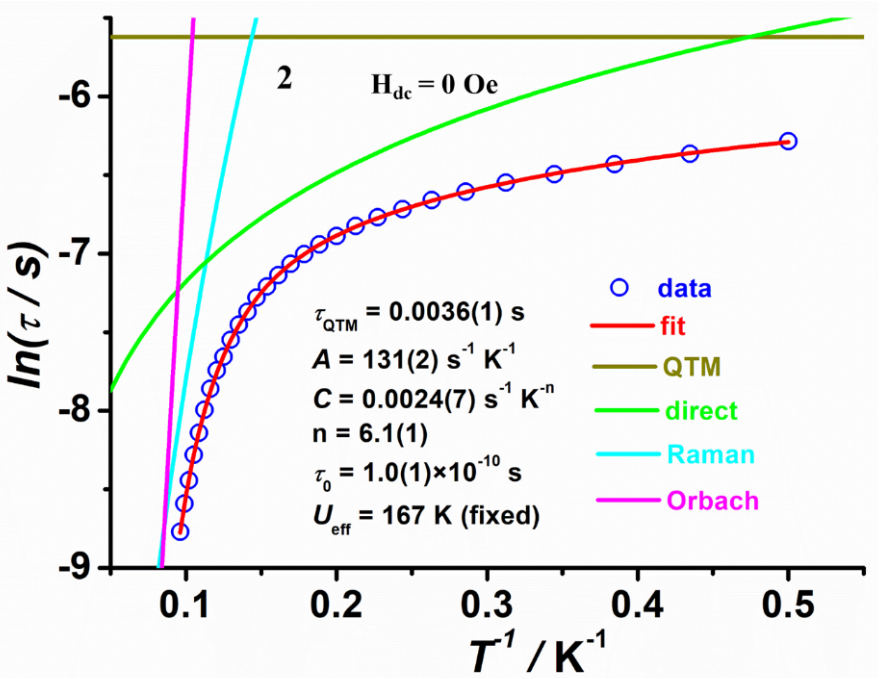

Figure S29. Relaxation time of the magnetization *ln(τ)* vs T^{-1} plot for complex **2** under 0 Oe dc field. The red solid line represents the best fit by the QTM, direct, Raman and Orbach processes. The other lines represent the individual contributions of the QTM (brown), direct (green), Raman (cyan) and Orbach (magenta) processes.

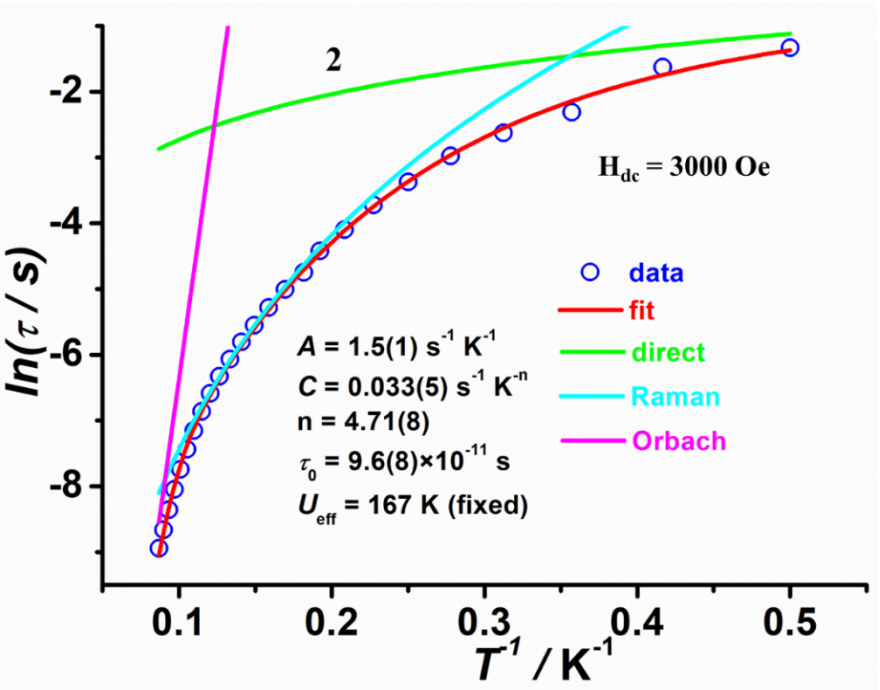

Figure S30. Relaxation time of the magnetization *ln(τ)* vs T^{-1} plot for complex **2** under 3000 Oe dc field. The red solid line represents the best fit by the direct, Raman and Orbach processes. The other lines represent the individual contributions of the direct (green), Raman (cyan) and Orbach (magenta) processes.

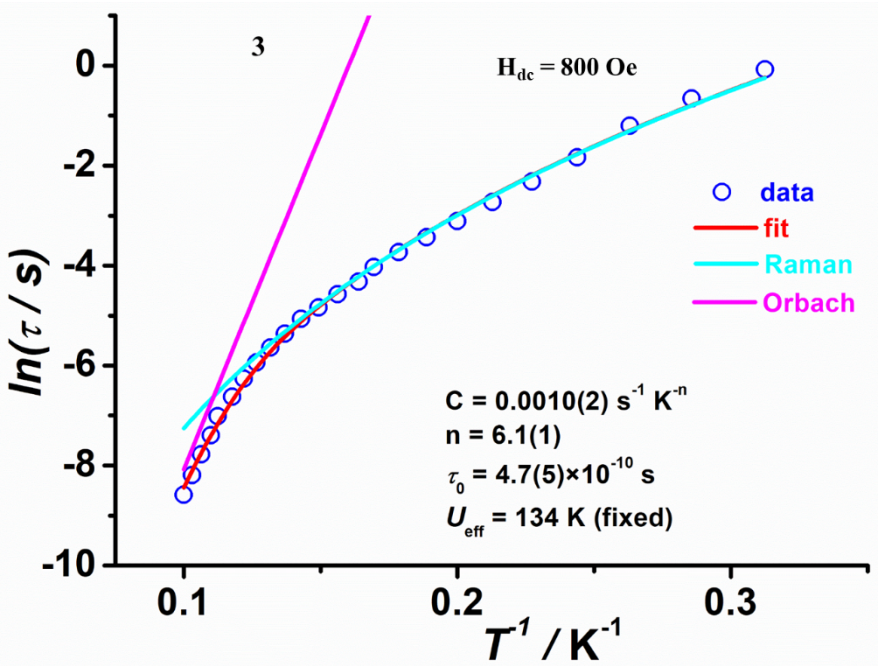

Figure S31. Relaxation time of the magnetization *ln(τ)* vs T^{-1} plot for complex **3** under 800 Oe dc field. The red solid line represents the best fit by the Raman and Orbach processes. The other lines represent the individual contributions of the Raman (cyan) and Orbach (magenta) processes.

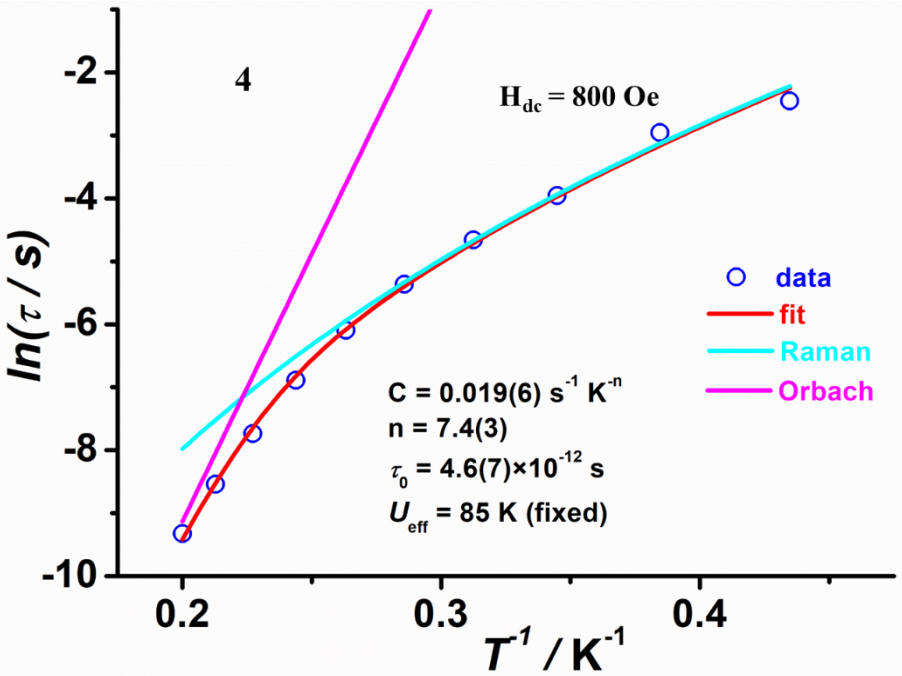

Figure S32. Relaxation time of the magnetization *ln(τ)* vs T^{-1} plot for complex **4** under 800 Oe dc field. The red solid line represents the best fit by the Raman and Orbach processes. The other lines represent the individual contributions of the Raman (cyan) and Orbach (magenta) processes.

Computational details

Based on the complete active space self-consistent field (CASSCF) and the N-electron valence second-order perturbation theory (NEVPT2) methods, *ab* initio

calculations were performed on the complexes **1**−**4**, to further understand the electronic structures and magnetic properties. Coordinates were obtained from the single-crystal X-ray diffraction experiments. Single-ion zero-field splittings for the complexes were calculated parameters *D*, *E* and *g* tensor. All calculations were performed under version 5.0.3 of the program ORCA.[S1] For CASSCF and NEVPT2 calculations, seven 3d electrons and five 3d orbitals of Co^{2+} ions were selected for the active space.[S2-S3] In the ZFS parameter calculations, 10 quartet and 40 doublet states were selected. Spin-orbit coupling was taken into consideration by using the quasi-degenerate perturbation theory (QDPT).[S4] Relativistic effects were accounted by using a second-order Douglas-Kroll-Hess (DKH2),[S5] and the CASSCF calculations are accelerated by RIJCOSX method.[S8]

Table S10. The CASSCF/NEVPT2/DKH-def2-TZVP computed individual contributions to the *D*-tensors of complexes **1**−**4**.

2S+1	Root	**1**			**2**		
		Energy / cm^{-1}	*D* / cm^{-1}	*E* / cm^{-1}	Energy / cm^{-1}	*D* / cm^{-1}	*E* / cm^{-1}
4	0	0	0.000	0.000	0	0.000	0.000
4	1	946.7	-96.105	0.000	1305.2	-76.733	0.005
4	2	6056.5	9.683	-9.684	6951.6	8.468	-8.340
4	3	7565.6	-0.001	-0.003	8487.1	0.008	0.008
4	4	9135.3	5.372	5.383	8538.3	6.962	6.862
2S+1	Root	**3**			**4**		
		Energy/cm^{-1}	*D* / cm^{-1}	*E* / cm^{-1}	Energy / cm^{-1}	*D* / cm^{-1}	*E* / cm^{-1}
4	0	0	0.000	0.000	0	0.000	0.000
4	1	2131.5	-70.101	0.001	2323.7	-47.454	-0.025
4	2	6691.9	11.933	-11.955	6343.3	9.079	-9.172
4	3	8588.7	0.507	0.506	8502.2	0.465	0.461
4	4	8727.5	8.222	8.234	8797.2	6.140	6.138

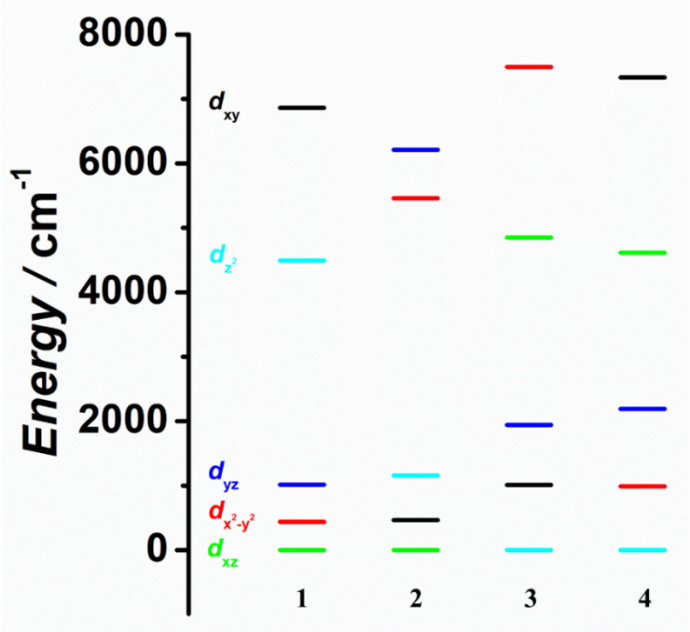

Figure S33. AILFT computed d-orbital energy diagram for complexes **1**–**4**.

Table S11. CASSCF computed electronic states, and the corresponding major electronic configurations for complexes **1**–**4**.

1		**2**	
Energy / cm^{-1}	Electronic configurations	Energy / cm^{-1}	Electronic configurations
0	$(d_{z^2})^1(d_{xz})^2(d_{yz})^1(d_{x^2-y^2})^2(d_{xy})^1$ (72 %) $(d_{z^2})^2(d_{xz})^2(d_{yz})^1(d_{x^2-y^2})^1(d_{xy})^1$ (22 %)	0	$(d_{z^2})^1(d_{xz})^2(d_{yz})^1(d_{x^2-y^2})^1(d_{xy})^2$ (38 %) $(d_{z^2})^1(d_{xz})^2(d_{yz})^1(d_{x^2-y^2})^2(d_{xy})^1$ (15 %) $(d_{z^2})^2(d_{xz})^2(d_{yz})^1(d_{x^2-y^2})^1(d_{xy})^1$ (14 %)
621.4	$(d_{z^2})^1(d_{xz})^2(d_{yz})^2(d_{x^2-y^2})^1(d_{xy})^1$ (44 %) $(d_{z^2})^1(d_{xz})^2(d_{yz})^1(d_{x^2-y^2})^1(d_{xy})^2$ (25 %) $(d_{z^2})^1(d_{xz})^1(d_{yz})^2(d_{x^2-y^2})^2(d_{xy})^1$ (18 %)	901.1	$(d_{z^2})^2(d_{xz})^1(d_{yz})^1(d_{x^2-y^2})^1(d_{xy})^2$ (53 %) $(d_{z^2})^2(d_{xz})^2(d_{yz})^1(d_{x^2-y^2})^2(d_{xy})^1$ (30 %)
4465.2	$(d_{z^2})^2(d_{xz})^1(d_{yz})^1(d_{x^2-y^2})^2(d_{xy})^1$ (95 %)	5133.5	$(d_{z^2})^1(d_{xz})^2(d_{yz})^1(d_{x^2-y^2})^2(d_{xy})^1$ (40 %) $(d_{z^2})^1(d_{xz})^2(d_{yz})^2(d_{x^2-y^2})^1(d_{xy})^1$ (23 %)
5394.9	$(d_{z^2})^1(d_{xz})^1(d_{yz})^2(d_{x^2-y^2})^2(d_{xy})^1$ (39 %) $(d_{z^2})^2(d_{xz})^1(d_{yz})^2(d_{x^2-y^2})^1(d_{xy})^1$ (28 %) $(d_{z^2})^2(d_{xz})^1(d_{yz})^1(d_{x^2-y^2})^1(d_{xy})^2$ (21 %)	6179.3	$(d_{z^2})^2(d_{xz})^1(d_{yz})^1(d_{x^2-y^2})^2(d_{xy})^1$ (44 %) $(d_{z^2})^1(d_{xz})^1(d_{yz})^2(d_{x^2-y^2})^1(d_{xy})^2$ (19 %) $(d_{z^2})^1(d_{xz})^2(d_{yz})^2(d_{x^2-y^2})^1(d_{xy})^1$ (10 %)
6702.6	$(d_{z^2})^1(d_{xz})^2(d_{yz})^1(d_{x^2-y^2})^1(d_{xy})^2$ (44 %) $(d_{z^2})^1(d_{xz})^2(d_{yz})^2(d_{x^2-y^2})^1(d_{xy})^1$ (19 %) $(d_{z^2})^1(d_{xz})^1(d_{yz})^2(d_{x^2-y^2})^1(d_{xy})^2$ (10 %)	6237.7	$(d_{z^2})^1(d_{xz})^2(d_{yz})^2(d_{x^2-y^2})^1(d_{xy})^1$ (39 %) $(d_{z^2})^1(d_{xz})^1(d_{yz})^2(d_{x^2-y^2})^1(d_{xy})^2$ (32 %) $(d_{z^2})^1(d_{xz})^2(d_{yz})^1(d_{x^2-y^2})^2(d_{xy})^1$ (14 %)
3		**4**	
Energy / cm^{-1}	Electronic configurations	Energy / cm^{-1}	Electronic configurations
0	$(d_{z^2})^2(d_{xz})^1(d_{yz})^1(d_{x^2-y^2})^1(d_{xy})^2$ (44 %) $(d_{z^2})^2(d_{xz})^1(d_{yz})^1(d_{x^2-y^2})^2(d_{xy})^1$ (41%)	0	$(d_{z^2})^2(d_{xz})^1(d_{yz})^1(d_{x^2-y^2})^2(d_{xy})^1$ (22 %) $(d_{z^2})^1(d_{xz})^2(d_{yz})^1(d_{x^2-y^2})^2(d_{xy})^1$ (22 %) $(d_{z^2})^2(d_{xz})^1(d_{yz})^1(d_{x^2-y^2})^1(d_{xy})^2$ (16 %)
1468.4	$(d_{z^2})^1(d_{xz})^1(d_{yz})^2(d_{x^2-y^2})^2(d_{xy})^1$ (25 %) $(d_{z^2})^1(d_{xz})^1(d_{yz})^2(d_{x^2-y^2})^1(d_{xy})^2$ (25 %) $(d_{z^2})^2(d_{xz})^1(d_{yz})^2(d_{x^2-y^2})^1(d_{xy})^1$ (22 %)	1522.5	$(d_{z^2})^1(d_{xz})^1(d_{yz})^2(d_{x^2-y^2})^1(d_{xy})^2$ (26 %) $(d_{z^2})^1(d_{xz})^2(d_{yz})^2(d_{x^2-y^2})^1(d_{xy})^1$ (17 %) $(d_{z^2})^1(d_{xz})^1(d_{yz})^2(d_{x^2-y^2})^2(d_{xy})^1$ (17 %)

			$(d_{z^2})^1(d_{xz})^1(d_{yz})^2(d_{x^2-y^2})^2(d_{xy})^1$ (16 %)
4911.5	$(d_{z^2})^1(d_{xz})^2(d_{yz})^1(d_{x^2-y^2})^1(d_{xy})^2$ (30 %) $(d_{z^2})^1(d_{xz})^2(d_{yz})^1(d_{x^2-y^2})^2(d_{xy})^1$ (26 %) $(d_{z^2})^2(d_{xz})^2(d_{yz})^1(d_{x^2-y^2})^1(d_{xy})^1$ (18 %)	4634.1	$(d_{z^2})^2(d_{xz})^1(d_{yz})^1(d_{x^2-y^2})^2(d_{xy})^1$ (25 %) $(d_{z^2})^1(d_{xz})^1(d_{yz})^2(d_{x^2-y^2})^2(d_{xy})^1$ (22 %) $(d_{z^2})^1(d_{xz})^2(d_{yz})^2(d_{x^2-y^2})^1(d_{xy})^1$ (16 %)
6215.3	$(d_{z^2})^1(d_{xz})^2(d_{yz})^2(d_{x^2-y^2})^1(d_{xy})^1$ (68 %) $(d_{z^2})^1(d_{xz})^1(d_{yz})^1(d_{x^2-y^2})^2(d_{xy})^2$ (14 %)	6077.6	$(d_{z^2})^2(d_{xz})^1(d_{yz})^2(d_{x^2-y^2})^1(d_{xy})^1$ (33 %) $(d_{z^2})^1(d_{xz})^2(d_{yz})^1(d_{x^2-y^2})^1(d_{xy})^2$ (24 %) $(d_{z^2})^1(d_{xz})^1(d_{yz})^2(d_{x^2-y^2})^2(d_{xy})^1$ (17 %)
6604.3	$(d_{z^2})^2(d_{xz})^1(d_{yz})^1(d_{x^2-y^2})^2(d_{xy})^1$ (36 %) $(d_{z^2})^2(d_{xz})^1(d_{yz})^1(d_{x^2-y^2})^1(d_{xy})^2$ (30 %) $(d_{z^2})^1(d_{xz})^1(d_{yz})^2(d_{x^2-y^2})^1(d_{xy})^2$ (13 %)	6657.1	$(d_{z^2})^2(d_{xz})^1(d_{yz})^1(d_{x^2-y^2})^1(d_{xy})^2$ (33 %) $(d_{z^2})^2(d_{xz})^1(d_{yz})^1(d_{x^2-y^2})^2(d_{xy})^1$ (14 %) $(d_{z^2})^2(d_{xz})^2(d_{yz})^1(d_{x^2-y^2})^1(d_{xy})^1$ (13 %) $(d_{z^2})^1(d_{xz})^2(d_{yz})^1(d_{x^2-y^2})^2(d_{xy})^1$ (13 %) $(d_{z^2})^1(d_{xz})^1(d_{yz})^2(d_{x^2-y^2})^1(d_{xy})^2$ (11 %)

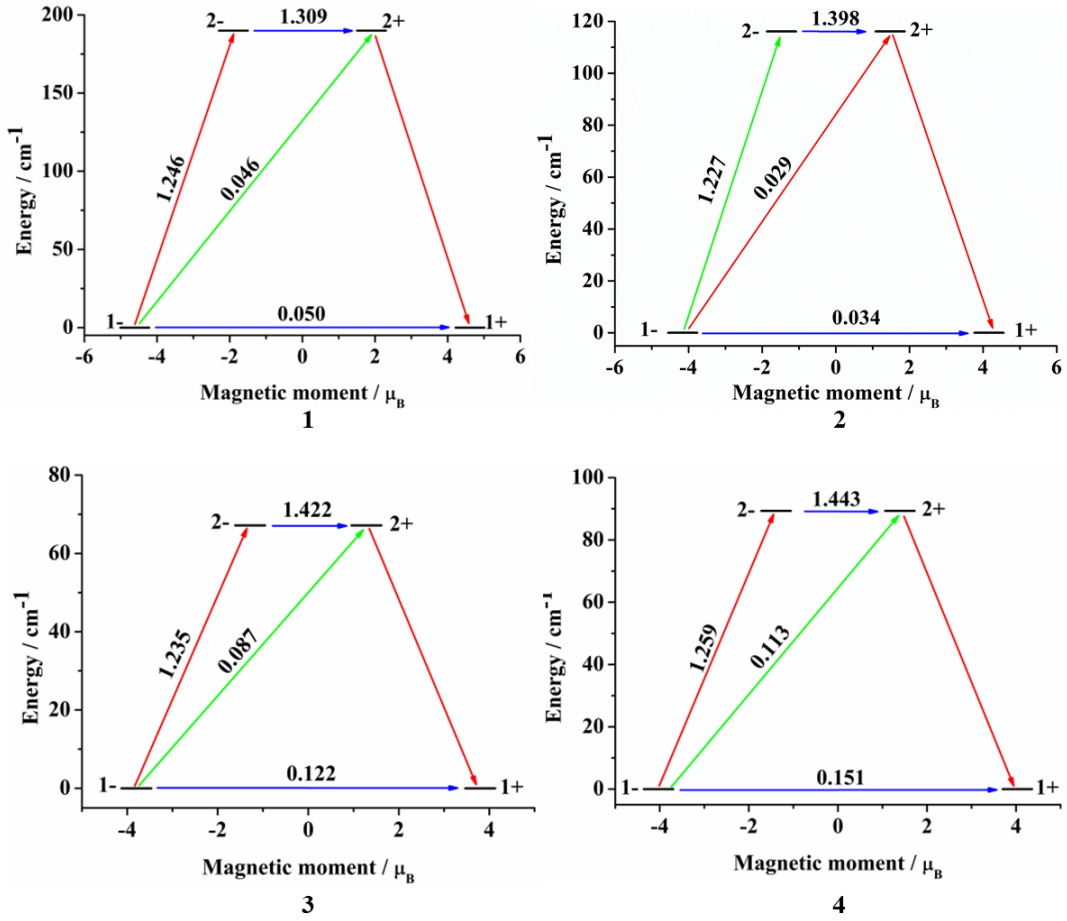

Figure S34. Lowest two KDs and *ab initio* calculated relaxation mechanism for complexes **1**–**4**. Thick black lines represent the KDs as a function of their magnetic moment along the principal anisotropy axis. Red lines indicate the mechanism of magnetization reversal. Blue lines correspond to the ground-state QTM and thermally assisted–QTM via the first excited KD, and green lines represent the possible Orbach relaxation process.

Table S12. Ab initio computed relative energies, principal values of the *g*-tensor of the four lowest Kramers doublets (KDs) for complexes **1**−**4**.

		1	**2**	**3**	**4**
KD_0	E	0.000	0.000	0.000	0.000
	g_x	0.1453	0.1019	0.3705	0.4316
	g_y	0.1532	0.1035	0.4016	0.4752
	g_z	9.2243	8.3168	8.1113	8.0560
KD_1	E	189.973	116.128	93.756	89.340
	g_x	3.8022	4.2668	4.6329	4.7027
	g_y	3.8543	4.1223	3.9956	3.9552
	g_z	4.0020	2.9472	2.8189	2.7819
KD_2	E	891.858	1459.030	1590.491	1638.229
	g_x	3.9773	4.2926	4.8268	4.7474
	g_y	3.9059	4.1232	3.9022	4.0289
	g_z	0.1792	1.0445	1.1311	1.1618
KD_3	E	1169.892	1640.988	1771.032	1816.306
	g_x	0.0148	0.0670	0.3508	0.2624
	g_y	0.0468	0.0798	0.3799	0.2933
	g_z	2.7368	3.6657	3.8238	3.8761

References

S1 (a) F. Neese, The ORCA program system, *Wiley Interdiscip. Rev.: Comput. Mol. Sci.*, 2012, **2**, 73−78, (b) F. Neese, Software update: the ORCA program system, version 4.0, *Wiley Interdiscip. Rev.: Comput. Mol.Sci.*, 2018, **8**, e1327. (c) F. Neese, F. Wennmohs, U. Becker and C. Riplinger, The ORCA quantum chemistry program package, *J. Chem. Phys.*, 2020, **152**, 224108. (d) F. Neese, ORCA-an Ab Initio, Density Functional and Semiempirical Program Package, 5.0.3, University of Bonn, Bonn, Germany, 2022, http://www.thch.uni-bonn.de/tc/orca/

S2 P. A. Malmqvist and B. O. Roos, The CASSCF state interaction method, *Chem. Phys. Lett.*, 1989, **155**, 189−194.

S3 (a) C. Angeli, R. Cimiraglia, S. Evangelisti, T. Leininger and J. P. Malrieu, Introduction of *n*-electron valence states for multireference perturbation theory, *J. Chem. Phys.*, 2001, **114**, 10252−10264. (b) C. Angeli, R. Cimiraglia and J. P. Malrieu, N-electron valence state perturbation theory: a fast implementation of the strongly contracted variant, *Chem. Phys. Lett.*, 2001, **350**, 297−305. (c) C. Angeli, R. Cimiraglia and J. P. Malrieu, n-electron valence state perturbation theory: A spinless formulation and an efficient implementation of the strongly contracted and of the partially contracted variants, *J. Chem. Phys.*, 2002, **117**, 9138−9153. (d) C. Angeli, S. Borini, M. Cestari and R. Cimiraglia, A quasidegenerate formulation of the second order n-electron valence state perturbation theory approach, *J. Chem. Phys.*, 2004, **121**, 4043−4049. (e) C. Angeli, B. Bories, A. Cavallini and R. Cimiraglia, Third-order multireference perturbation theory: The n-electron valence state perturbation-theory approach, *J. Chem. Phys.*, 2006, **124**, 054108. (f) R. Herchel, I. Nemec, M. Machata and Z. Trávníček, Solvent-induced structural diversity in tetranuclear Ni(ii)

Schiff-base complexes: the first Ni_4 single-molecule magnet with a defective dicubane-like topology, *Dalton Trans.*, 2016, **45**, 18622−18634.

S4 D. Ganyushin and F. Neese, First-principles calculations of zero-field splitting parameters, *J. Chem. Phys.*, 2006, **125**, 024103.

S5 I. Malkin, O. L. Malkina, V. G. Malkin and M. Kaupp, Scalar relativistic calculations of hyperfine coupling tensors using the Douglas-Kroll-Hess method, *Chem. Phys. Lett.*, 2004, **396**, 268−276.

S6 F. Weigend and R. Ahlrichs, Balanced basis sets of split valence, triple zeta valence and quadruple zeta valence quality for H to Rn: Design and assessment of accuracy, *Phys. Chem. Chem. Phys.*, 2005, **7**, 3297−3305.

S7 F. Weigend, Accurate Coulomb-fitting basis sets for H to Rn, *Phys. Chem. Chem. Phys.*, 2006, **8**, 1057−1065.

S8 F. Neese, F. Wennmohs, A. Hansen and U. Becker, Efficient, approximate and parallel Hartree-Fock and hybrid DFT calculations. A 'chain-of-spheres' algorithm for the Hartree-Fock exchange, *Chem. Phys.*, 2009, **356**, 98−109. (b) R. Izsak and F. Neese, An overlap fitted chain of spheres exchange method, *J. Chem. Phys.*, 2011, **135**, 144105.